UC Irvine
UC Irvine Previously Published Works

Title
GSTM1 Deficiency Exacerbates Cisplatin-Induced Kidney Injury via Increased Oxidative Stress.

Permalink
https://escholarship.org/uc/item/66q0z9s9

Journal
Clin Sci (Lond)

ISSN
0143-5221

Authors
Chen, Luojing
Ayon, Ramon J
Mekhaiel, Karen E
et al.

Publication Date
2026-11-13

DOI
10.1042/CS20250134

Peer reviewed

eScholarship.org Powered by the California Digital Library
University of California

GSTM1 Deficiency Exacerbates Cisplatin-Induced Kidney Injury via Increased Oxidative Stress

Luojing Chen [1*], Ramon Ayon [2*], Karen E. Mekhaiel [2], Timothy Beane [1], Yitong Zhao [2], Yuzana Mone [2], Yves Wang [1], Ahmed Alnuaimi [1], Phillip Ruiz [3], and Thu H. Le [1,2]

[1]Department of Medicine, Division of Nephrology, University of Rochester Medical Center Rochester, NY;

[2]Department of Medicine, Division of Nephrology, University of California, Irvine, Irvine, CA

[3]Department of Pathology, University of Miami, Miami, Florida

**These two authors have equal contributions.*

Corresponding author:
Thu H. Le, MD
Department of Medicine, Division of Nephrology
UCI School of Medicine
101 The City Drive South
@City Tower Building – Suite 400
Orange, CA
Email: thuhl@hs.uci.edu

Abstract

Cisplatin, a potent chemotherapeutic agent, is highly effective in various cancers but its use is significantly limited by kidney injury, occurring in approximately 30% of patients. Cisplatin-induced kidney injury compromises optimal dosing, reducing cancer survival, and leads to permanent eGFR decline, increasing chronic kidney disease (CKD) risk and cardiovascular mortality. Increased reactive oxygen species (ROS) generation is central to cisplatin nephrotoxicity. Glutathione-S-transferase Mu-1 (GSTM1), a phase II detoxification enzyme, protects against oxidative stress. A common *GSTM1* null deletion variant is highly prevalent in human populations. We hypothesized that *GSTM1* deficiency increases susceptibility to cisplatin nephrotoxicity. Using a clinically relevant low-dose, repeat-cycle cisplatin mouse model, we found that cisplatin treatment significantly induces renal *Gstm1* expression in wild-type mice, suggesting a protective role. *Gstm1* knockout mice exhibited more severe kidney injury, evidenced by elevated creatinine, BUN, KIM-1, 4-HNE adducts, and histological damage. This exacerbated injury was associated with significantly higher renal ROS and NOX2 expression and mitochondrial ROS. *In vitro studies* using primary mouse proximal tubular cells deficient in *Gstm1* and human HK-2 cells endogenously lacking *GSTM1* demonstrated that GSTM1 deficiency leads to increased mitochondrial ROS and NOX2 expression following cisplatin treatment; conversely, overexpression of *GSTM1* in HK-2 cells significantly attenuated cisplatin-induced mitochondrial ROS and NOX2 expression. Furthermore, GSTM1 protected against NF-κB activation and cell death. Our findings establish GSTM1 as a critical cytoprotective factor against cisplatin nephrotoxicity, mitigating oxidative stress, inflammation, and apoptosis, and identify the highly prevalent *GSTM1* null variant as a potential genetic risk factor for cisplatin-induced kidney injury.

Introduction

Cisplatin is a highly effective chemotherapeutic agent used to treat a variety of cancers, including those of the head and neck, ovary, lung, cervix, endometrium, and bladder. Its efficacy is particularly remarkable in metastatic testicular cancer, where there is ~ 80% cure rate (1). However, a significant limitation to its widespread use is its considerable toxicity, notably kidney injury, which occurs in up to 30% of patients receiving cisplatin and accounts for as much as 20% of all kidney injury episodes in hospitalized cancer patients (2, 3).

The occurrence of cisplatin-induced kidney injury often necessitates a reduction in the optimal cumulative dose of cisplatin, which, in turn, can significantly compromise overall cancer survival (e.g., a drop from 74% to 51%). Furthermore, cisplatin-induced kidney injury has long-term implications for chronic kidney disease (CKD). Patients who experience cisplatin-induced kidney injury often exhibit a permanent decline in estimated glomerular filtration rate (eGFR) (4, 5), leading to increased risks of CKD progression, cardiovascular complications, and mortality.

Increased reactive oxygen species (ROS) generation is a well-established key player in cisplatin nephrotoxicity (6, 7). Glutathione-S-transferases (GSTs) are a superfamily of phase II detoxification enzymes that provide crucial cytoprotection against oxidative stress. Among the thirteen distinct classes of soluble GSTs identified (8-10), Glutathione-S-transferase Mu-1 (GSTM1), encoded by the *GSTM1* gene, is one of five mu (μ) class GST enzymes in humans and is evolutionarily conserved (11). It plays a vital role in detoxifying electrophilic compounds.

It should be noted that the GST mu gene family has undergone lineage-specific duplications in mammals; while mouse *Gstm1* and human *GSTM1* share a common ancestral origin and high amino acid sequence identity (~80%), they are not strict 1:1 orthologs. Nevertheless, mouse *Gstm1* represents the functionally analogous Mu-class enzyme in the kidney and serves as an established model for studying the consequences of human GSTM1 deficiency.

A common null deletion variant of *GSTM1* is highly prevalent across human populations, affecting up to 50% of Caucasians and Asians and 27% of African Americans who are homozygous carriers. *GSTM1* null variant has been associated with CKD progression (12-16) and incident end stage kidney disease (17). Studies in *Gstm1* knockout (KO) mice have shown increased oxidative stress and heightened susceptibility to kidney injury in models of chronic kidney disease (18). However, the role of GSTM1 in cisplatin-induced kidney injury is unknown. A recent study reported that mice with combined deletion of *Gstt1* and *Gstm1* genes exhibited more severe kidney injury and oxidative stress three days after a single high dose of cisplatin (20 mg/kg) (19). However, the clinical relevance of this high-dose single-administration model to human treatment regimen, which typically involves repeated dosing cycles, has been questioned.

We hypothesize that *GSTM1* deficiency alone is sufficient to increase susceptibility to cisplatin nephrotoxicity. Here, we evaluate the impact of *Gstm1* gene deletion on kidney function and pathology using a low-dose cisplatin kidney injury model that more closely mimics the dose regimen of cisplatin in human patients.

Methods

Animal Model

Experiments were conducted in accordance with local and National Institutes of Health (NIH) guidelines, and the animal protocol received approval from the University of Rochester and University of California, Irvine Institutional Animal Care and Use Committees. The mouse line carrying the *Gstm1* deletion was generated by electroporation of embryonic stem cells derived from the 129/SvEv (129S6, Taconic) strain with a targeting construct designed to disrupt a 21 kb segment of the *Gstm1* locus, as previously described (18). This line was subsequently backcrossed onto the FVB background for over 20 generations. All mice were housed under a

12-hour light-dark cycle with *ad libitum* access to standard chow and water. All animal experiments were conducted at the University of Rochester Medical Center and University of California, Irvine. Since our colony is maintained using heterozygous (*Gstm1 +/-*) breeding pairs, the number of wild-type (+/+) and knockout (-/-) littermates available from any single litter is inherently limited by Mendelian inheritance ratios. To achieve the desired group sizes while maintaining the use of age-matched littermate controls, animals were pooled across three independent cohorts of littermates bred at different times, with all mice within the same age range (8–12 weeks) at the time of cisplatin treatment. This approach of three independent experiments also served to confirm the reproducibility of our findings across distinct animal cohorts.

Cisplatin Nephrotoxicity Model

Cisplatin (Cat number: D3371) was purchased from Tokyo Chemical Industry and freshly prepared in sterile 0.9% sodium chloride (saline) at 1 mg/mL. Male mice, aged 8–12 weeks, received 9 mg/kg cisplatin via intraperitoneal injection weekly for four consecutive weeks (Figure 1). The repeated low-dose cisplatin model was employed because it more closely recapitulates the repeated dosing cycles administered to human cancer patients than acute single high-dose models (typically 20–25 mg/kg) and has been shown to produce progressive chronic kidney disease (20). The dose of 9 mg/kg was selected based on pilot experiments in which this dose produced more consistent and detectable elevations in plasma creatinine and BUN at one-month post-final injection compared to lower doses of 3 mg/kg and 7 mg/kg in our FVB colony. The Week 8 time point (four weeks after the fourth and final cisplatin dose) was chosen to allow sufficient interval for functional markers of chronic kidney injury to become robustly elevated above baseline while reducing the influence of acute post-injection toxicity. At the end of the eighth week after the first injection (four weeks after the fourth and final injection), plasma was collected. A 10 µL aliquot was sent to the UAB-UCSD O'Brien Center for Acute Kidney Injury

Research for creatinine measurement using gold-standard mass spectrometry. Blood urea nitrogen (BUN) levels were determined using a BUN Colorimetric Detection Kit (Cat. K024-H1, ARBOR ASSAY, Ann Arbor, Michigan), following the manufacturer's protocol. Data were analyzed using GraphPad Prism 10.2.0 software (GraphPad Software, San Diego, CA, USA). Kidney tissues were collected for RNA analysis, fluorescence-activated cell sorting (FACS), and histology (See Figure 1A).

In vitro experiments

Generation of HK-2 Proximal Tubular Cell Line (PTCL) Expressing Human GSTM1

HK-2 cells (American Type Culture Collection, Manassas, VA, Cat. CRL-2190), a proximal tubule cell line (PTCL) derived from a normal human adult male kidney, do not endogenously express GSTM1 (confirmed by qPCR and Western blot analysis). We therefore introduced cDNA encoding a full-length human *GSTM1* gene (NM_000561.4, GenScript, Piscataway, NJ) into HK-2 cells. The human *GSTM1* gene was cloned into a pLenti-vector (GenScript) at the EcoRI/NheI cloning sites, with expression driven by a CMV promoter. A stable HK-2-GSTM1 cell line (HK-2-Tg) was established through puromycin (1 mg/mL) selection for 10 days, and GSTM1 expression was confirmed by Western blot (see Supplemental Methods). HK-2 cells containing the pLenti-vector alone served as the control cell line (HK-2-control).

Control and Tg HK-2 cells were cultured in Keratinocyte Serum Free Medium (K-SFM) (Cat: 17005-042 from Thermo Fisher Scientific) at 37 °C and 5% CO2. After treatment with or without apocynin (100 μM) (Cat. sc-203321A, Santa Cruz Biotech) for 18 hours, cells were then incubated with 30 μM cisplatin for 24 hours or 48 hours as indicated in specific experiments.

Isolation, Culture, and Cisplatin Exposure of Primary Proximal Tubular Epithelial Cells (PTECs)

Mouse PTECs were isolated from kidneys of WT and *Gstm1* KO mice aged 4–6 weeks as previously described (21) and grown on precoated plates in DMEM/F-12 medium supplemented with 10% FBS, non-essential amino acids, and insulin-transferrin-selenium. At approximately 90% confluence, cells were split, and an equal number of WT-PTEC and KO-PTEC were plated on new coated plates for 24 hours, followed by treatment with cisplatin (20 μM) for 24 hours.

Detection of Cell Death

Flow Cytometry

The number of apoptotic proximal tubular cells treated with cisplatin was detected by flow cytometric analysis using the Annexin V Apoptosis Detection Kit (Cat. 88-8102-72, Thermo Fisher Scientific). One million (1×10^6) HK-2-control and HK-2-Tg cells treated with 30 μM cisplatin were used for the apoptosis assay, following the manufacturer's instructions. Briefly, cells were trypsinized for 5 minutes and centrifuged at 1500 rpm. Cells were suspended in Annexin V buffer, and 1×10^6 cells were stained with 5 μL Annexin for 15 minutes at 4 °C, followed by 7-AAD stain for 5 minutes at 4 °C in the dark. Samples were immediately analyzed by FACS at the University of Rochester Medical School Core facility. Cells were classified as viable (Annexin $V^{-/}$7-AAD^-; Q4), early apoptotic (Annexin V^+/7-AAD^-; Q3), late apoptotic/necrotic (Annex V^+/7-AAD^+; Q2), or membrane-compromised cells without detectable Annexin V staining (Annexin V^-/7-AAD^+; Q1). The combined percentage of cells in Q2 and Q3 was reported as %apoptotic cells. Results were analyzed using FlowJo 10.10 software.

TUNEL Assay

The TUNEL assay was employed to detect kidney apoptosis induced by cisplatin. WT and *Gstm1* KO mice were treated with 9 mg/kg cisplatin as described above. At the end of the experiment, kidneys were fixed and embedded in paraffin, then cut into 4-μm sections/slides. Standard dewaxing/rehydration was performed, followed by permeabilization with 0.5% Triton-X

in PBS for 10 minutes. After a quick wash with PBS, TUNEL staining was performed with the TUNEL stain kit (Sigma/Roche, Cat. 12156792910) following the manufacturer's protocol, followed by nuclear staining with DAPI. Images were captured with a fluorescence microscope (Olympus BX51). Positive nuclear TUNEL staining was represented as the number of positive TUNEL stained cells per field. A total of 150 or more nuclei from five random fields were counted and similar results were obtained from two independent experiments.

Measurement of Reactive Oxygen Species (ROS)

Intracellular ROS production was detected using the Reactive Oxygen Species Assay Kit (ab113851, Abcam), following the manufacturer's instructions. Briefly, HK-2 control and HK-2-Tg cells were exposed to cisplatin (30 μM) for 24 hours in the absence or presence of the NADPH oxidase inhibitor apocynin (Apo) (100 μM). Cells were then stained with 10 μM DCFDA solution for 40 minutes at 37 °C, protected from light. Intracellular ROS production was measured using a plate reader (Bio-Tec Instruments, Inc) at Ex-485 nm and Em-535 nm. The relative level of ROS production is shown as fold of the control. Data are expressed as mean ± SEM.

To detect ROS production in cisplatin-treated mouse kidneys, 2 mg of kidney tissue was mashed with the end of a 3ml syringe for approximately 1-2 minutes in 250 μL DCFDA buffer. 10 μM DCFDA solution was then added and incubated at 37 °C for 30 minutes. Intracellular ROS production was measured at Ex-485 nm and Em-535 nm. The relative level of ROS production is shown as fold of the WT mice treated with cisplatin.

To detect mitochondrial superoxide levels, the MitoSOX Red probe (Cat. M36007, Thermo Fisher Scientific) was used. Briefly, approximately 3 x 10^5 cells/well in a 6-well plate of HK-2 control and HK-2-Tg cells were treated with 30 μM cisplatin for 24 hours. 1 μM MitoSOX Red probe was added to both cisplatin-treated and untreated cells for 60 minutes. Cells were then analyzed either with a BD LSRII flow cytometer (University of Rochester Medical Center core

facility) or imaged with an inverted fluorescence microscope (Olympus IX71). Arbitrary units of MitoSOX Red intensity were calculated with ImageJ. Five random fields were used for ImageJ analysis. Similarly, the MitoSOX Red probe was used for detection of mitochondrial superoxide level for PTECs. Approximately 3 x 10^5 cells/well in a 6-well plate of WT-PTEC and *Gstm1* KO-PTEC cells were treated with 20 μM cisplatin for 20 hours. MitoSOX Red intensity was analyzed by ImageJ and expressed as arbitrary units. Two independent experiments were performed.

Tissue Preparation and Histology

Tissue preparation was performed at the core facility at the University of Rochester Medical Center. For paraffin sections, kidneys were first fixed with 4% paraformaldehyde and embedded in paraffin. Paraffin-embedded tissues were cut into 4-μm sections. PAS and Masson's trichrome staining were performed according to standard procedures. Kidney histology was examined on formalin sections stained with PAS and Masson's trichrome by a pathologist blinded to experimental conditions and genotypes as previously described (22).

Immunohistochemistry

Immunohistochemistry staining was performed using the ImmPACT DAB EqV Substrate Kit (Cat. SK-4013, Peroxidase, Vector Laboratory), following the company's instructions. After standard deparaffinization, sections were placed in citrate-buffered solution (pH 6.0) and boiled for 10 minutes to retrieve antigens. Endogenous peroxidase was quenched with 3.0% hydrogen peroxide in methanol for 20 minutes. After blocking for 30 minutes using 3.0% bovine serum albumin (BSA, phosphate-buffered saline (PBS)), sections were incubated with one of the following primary antibodies: Anti-GSTM1 (400x dilution), Anti-KIM-1 (200x dilution), followed by incubation with HRP-conjugated secondary antibodies (MP-7401 - ImmPRESS Horse Anti-Rabbit IgG Polymer Kit or MP-7422 - ImmPRESS Horse Anti-Mouse IgG Polymer Kit, Peroxidase) for 40 minutes. Hematoxylin was used for counterstaining. Images were taken

(Olympus BX51) and quantified with ImageJ. Results were presented as the percentage of the positively stained area over the negative stain area. Five random fields were used for each group, and similar results were obtained from two independent experiments. Note: Due to the high degree of amino acid sequence homology between GSTM1 and GSTM2, cross-reactivity of the anti-GSTM1 antibody with GSTM2 cannot be excluded, and the immunohistochemical signal may therefore reflect combined Mu-class GST expression rather than GSTM1 exclusively.

NF-κB p65 Immunofluorescence Staining

For NF-κB p65 staining, approximately 1 x 10^5 cells/well in a 12-well plate of HK-2 control and HK-2-Tg cells grown on coverslips were treated with 30 μM cisplatin for 20 hours. Cells were then fixed with 4% paraformaldehyde, permeabilized with 0.2% Triton X-100 for 5 minutes, washed, and then stained with anti-p65 antibody (Cell Signaling Technology, Cat #3033) for 4 hours at room temperature. After 2 washes with PBS, cells were stained with Alexa Fluor-488-conjugated anti-Rabbit secondary antibody. After a final wash, nuclei were stained with DAPI (Sigma-Aldrich). Images were taken with a fluorescence microscope (Olympus BX51). NF-κB p65 nuclear staining was quantified as the percentage of p65 nuclei-positively stained cells over the total number of cells per field. A total of 150 or more nuclei from five random fields were counted for each group, and similar results were obtained from two independent experiments.

RNA Extraction and Real-time Quantitative PCR

Total RNA isolation was performed as previously described. Briefly, total RNA was extracted from the kidneys using TRIzol (Thermo Fisher Scientific) and a RNeasy Mini Kit (Qiagen, Hilden, Germany). 200 ng RNA was used for cDNA synthesis, and quantitative real-time PCR was performed using SYBR Green Supermix (BioRad, Hercules, CA). Quantification of PCR products was done using the comparative cycle threshold method as described previously (23). *Gapdh* was used as an internal control to determine the relative expression of each gene.

Sequences of all qPCR primers (mouse (m) and human (h)) are summarized in **Supplemental Table 1**.

Western blot

Kidney tissues were homogenized in RIPA lysis buffer (Thermo Fisher; 89900) supplemented with Halt inhibitor cocktail (Thermo Fisher; 78440). Protein concentrations were determined using a Pierce™ BCA protein assay Thermo Fisher; A65453), and 30 µg of protein per sample was separated by SDS-PAGE and transferred to membranes. Membranes were blocked using EveryBlot Blocking Buffer (Bio-Rad; 12010020) and incubated with antibodies against 4-HNE (R&D Systems, MAB3249; 1:1,000) and GAPDH (Cell Signaling Technology; 2118; 1:3,000). Membranes were subsequently incubated with the appropriate HRP-conjugated secondary antibodies (Bio-Rad). Protein signals were developed using Clarity Western ECL Substrate (Bio-Rad; 1705060) and imaged using a ChemiDoc MP Imaging System (Bio-Rad). The total 4-HNE protein-adduct signal across each lane was quantified using ImageJ, normalized to the corresponding GAPDH signal, and expressed as fold change relative to cisplatin-treated wild-type mice.

Statistical Analysis

All experiments were performed at least twice independently. All data were expressed as mean ± SEM, and GraphPad Prism 10.2.0 software (GraphPad software, San Diego, CA, USA) was used to perform statistical analyses. When comparing two groups, two-tailed, unpaired Student's t tests (nonparametric test and Mann-Whitney test) were applied to indicate statistical significance (p-value less than 0.05 was considered significant difference).

Results

Kidney *Gstm1* Gene Expression is Induced After Cisplatin Treatment in a Low-Dose Cisplatin Mouse Model

To first determine whether *Gstm1* plays a role in cisplatin nephrotoxicity, we utilized an established mouse model involving repeat low-dose cisplatin treatment that closely mimics the human clinical dosing regimen. Wild-type mice were treated with cisplatin at 9 mg/kg once a week for four weeks. As shown in **Figure 1A**, at the end of eight weeks after the first dose of cisplatin (or four weeks after the 4th and final dose), renal *Gstm1* expression was compared between wild-type control mice (no cisplatin treatment) and wild-type mice treated with cisplatin. As depicted in **Figure 1B**, renal *Gstm1* mRNA expression was significantly elevated (approximately 4-fold) in cisplatin-treated wild-type mice compared to untreated wild-type mice. In the mouse kidney, by immunohistochemistry, compared to saline-treatment, cisplatin treatment induced significant increase in GSTM1 protein expression primarily in the juxtamedullary cortex and outer medullary region (**Figure 1C**), an area most vulnerable to cisplatin-induced injury due to the high metabolic activity, active cisplatin uptake via organic cation transporters. This suggests that the observed increase in *Gstm1* may represent a protective response to cisplatin-induced injury.

Deletion of *Gstm1* Leads to More Severe Cisplatin-Induced Kidney Injury

Next, to determine if increased *Gstm1* expression in mice confers a protective role against cisplatin-induced kidney injury, wild-type and *Gstm1* knockout (KO) mice were treated with cisplatin weekly for four weeks. At the end of the eighth week after the first dose, plasma creatinine and BUN levels were significantly higher in *Gstm1* KO mice (**Figure 2A**). Plasma creatinine and BUN measurements from saline treated wild-type mice were included for comparison. Consistent with these findings, renal expression of kidney injury molecule-1 (KIM-1) (**Figure 2B**) was significantly increased in *Gstm1* KO mice, indicating that loss of GSTM1 increases susceptibility to cisplatin-induced renal tubular injury. Moreover, renal histopathology scores were significantly higher in *Gstm1* KO mice, with the most striking histological difference

in tubular cast formation (yellow arrow, **Figure 2C**). Masson Trichome staining was very mild and not significantly different between the two groups (data not shown).

Gstm1 Deletion is Associated with Higher ROS Production in *Gstm1* KO Mouse Kidneys in Response to Cisplatin

The mechanisms underlying cisplatin-induced kidney damage are complex, and it is well-reported that cisplatin exposure leads to increased kidney ROS production (6, 7). Given GSTM1's important role in ROS signaling, we assessed markers of oxidative stress and inflammation to determine possible mechanisms of injury. By DCFDA assay and 4-HNE immunoreactivity, significantly higher levels of reactive oxygen species (ROS) and 4-HNE protein adducts were observed in *Gstm1* KO mice. (**Figure 3A** and **3B)**, respectively. This was associated with significantly higher renal expression of NOX2 and a trend toward higher expression of NOX4 (**Figure 3C**). While IL-6 expression was significantly increased in *Gstm1* KO mice, expression levels of IL-10, MCP-1, and TGF-β did not differ significantly between *Gstm1* KO mice and WT mice (**Figure 3C**). These findings suggest that GSTM1 plays a protective role by mitigating oxidative stress in cisplatin-induced nephrotoxicity.

Cisplatin is known to induce mitochondrial oxidative stress (24). Although GSTM1 is localized in the cytoplasm, we hypothesized that GSTM1 deficiency increases renal tubular mitochondrial ROS. Primary mouse proximal tubular cells (PTECs) were isolated, cultured, and treated with cisplatin (20 μM) for 24 hours. As shown in **Figure 3D,** at baseline, minimal MitoSOX Red staining was observed in both WT and *Gstm1* KO PTECs. After cisplatin treatment, MitoSOX Red intensity significantly increased in both genotypes compared to untreated cells, and was doubled in KO compared to WT PTECs. By illustrative FACS analysis, the percentage of cells positive for MitoSOX Red was higher in *Gstm1* KO PTECs after cisplatin treatment compared to WT (**Figure 3E**).

Overexpression of GSTM1 in Human HK-2 Cells Results in Lower ROS Production in Response to Cisplatin Treatment

To determine whether the re-introduction of GSTM1 protects from cisplatin-induced renal tubular injury, we transfected a human immortalized HK-2 proximal tubular cell line endogenously deficient in GSTM1, reflecting the highly prevalent homozygous genotype of the *GSTM1* null variant across human populations. **Supplemental Figure 1** demonstrates successful overexpression of GSTM1 in HK-2 cells carrying the human *GSTM1* transgene (Tg) by Western blot analysis. Similar to mouse primary PTECs, HK-2 control cells deficient in GSTM1 exhibited significantly higher ROS levels after exposure to cisplatin compared to HK-2 Tg cells expressing GSTM1 (**Figure 4A**). Moreover, consistent with the higher ROS level, human NOX2 expression was significantly increased in HK-2 control cells (**Figure 4B**). Treatment with apocynin, an inhibitor of NADPH oxidase, significantly reduced ROS levels in both cell lines compared to cisplatin alone (**Figure 4A**). Furthermore, similar to *Gstm1* KO primary mouse proximal tubular cells, the intensity of MitoSOX Red staining after cisplatin exposure was significantly lower in HK-2 Tg cells expressing GSTM1 (**Figure 4C**) and, by illustrative FACS analysis, HK-2 Tg cells had a lower percentage of MitoSOX Red positive cells (**Figure 4D**). Taken together, these findings suggest that GSTM1 is cytoprotective against cisplatin by decreasing NOX2 expression and, consequently, the generation of ROS.

Deletion of *Gstm1* Leads to an Increase in Cisplatin-Induced Cytotoxicity

It is generally accepted that cisplatin-induced toxicities include activation of the NF-κB signaling pathway, and inhibition of NF-κB has been shown to preserve renal function in mice (25). As shown in **Figure 5A**, GSTM1-deficient HK-2 control cells exhibited significantly higher NF-κB p65 nuclear translocation following cisplatin treatment compared to GSTM1-expressing HK-2-Tg cells, indicating that GSTM1 protects human proximal tubular cells against cisplatin-induced NF-κB activation *in vitro*. Importantly, this finding is directly and mechanistically linked to our *in vivo*

mouse data, where *Gstm1* knockout kidneys exhibit significantly elevated IL-6 mRNA expression compared to wild-type kidneys following cisplatin treatment (**Figure 3C**). IL-6 is one of the most well-validated downstream transcriptional targets of NF-κB signaling, and its upregulation in *Gstm1* knockout kidneys *in vivo* is consistent with, and can be mechanistically explained by, the increased NF-κB activation observed in GSTM1-deficient human proximal tubular cells *in vitro*. Together, the NF-κB p65 and IL-6 data provide biologically plausible mechanistic bridge between our human cell and mouse *in vivo* datasets through the NF-κB-IL-6 inflammatory axis, and represent a relevant link between these two experimental systems at the chronic injury time point.

Furthermore, illustrative Annexin V/7-AAD flow cytometry (**Figure 5B**) demonstrates that GSTM1-deficient HK-2 control cells exhibit higher rates of apoptotic cells (Annexin V^+/7-AAD^-, Q3) and late apoptosis/necrotic cells (Annexin V^+/7-AAD^+, Q2), following acute cisplatin exposure compared to GSTM1-expressing HK-2-Tg cells. The percentage of membrane-compromised cells without detectable Annexin V staining (Annexin V^-/7-AAD^+, Q1) is also higher in GSTM1-deficient HK-2 cisplatin-treated cells. The bar graph (**Figure 5B**, right) quantifies the combined percentage of Annexin V-positive cells in Q2 + Q3, encompassing the early apoptotic and late apoptotic/necrotic population. TUNEL staining (**Figure 5C**) demonstrates increased DNA fragmentation in *Gstm1* knockout kidneys compared to wild-type kidneys following chronic repeated low-dose cisplatin treatment, whereas there was virtually no TUNEL staining in either group with repeated saline treatment, reflecting the cumulative and distributed cell death burden that accumulates gradually over weeks of repeated cisplatin exposure. In this chronic model, only a small fraction of cells actively undergo DNA fragmentation at any single time point, consistent with the subclinical and progressive nature of injury, in contrast to the robust and synchronized apoptotic signal characteristic of acute high-dose cisplatin models. Despite representing different injury contexts and time scales, both the *in vitro* Annexin V data and the *in*

vivo TUNEL data consistently support the overarching conclusion that GSTM1 deficiency increases susceptibility to cisplatin-induced cell death, whether in the acute human cell model or the chronic *in vivo* mouse model.

Discussion

Cisplatin-based chemotherapy frequently leads to kidney injury, with a prevalence of approximately 30%. Despite this high incidence, there remains a critical lack of predictive tools and effective preventative measures for cisplatin-induced kidney injury. Furthermore, the genetic risk factors predisposing individuals to cisplatin-induced kidney injury have been largely underexplored. The common *GSTM1* null or deletion variant has been associated with CKD progression in humans. In mice, *Gstm1* deletion exacerbates kidney injury in models of hypertension and CKD. However, its specific role in cisplatin-induced kidney injury has been poorly investigated.

Here, we provide evidence that cisplatin exposure significantly increases renal *GSTM1* expression, suggesting a protective role for GSTM1 against cisplatin-induced cytotoxicity. Utilizing a *Gstm1* knockout mouse model that faithfully mimics the 21 kb gene deletion variant occurring in humans, we demonstrate that GSTM1 deficiency markedly exacerbates kidney injury in mice exposed to a clinically relevant chronic low-dose cisplatin regimen. This finding is particularly significant because it addresses a critical gap in the existing literature, which has primarily relied on acute, high-dose cisplatin models with questionable clinical translation. Our use of a chronic, low-dose model provides a more accurate representation of the repeated dosing cycles administered to human patients, thereby strengthening the clinical relevance of our findings.

The underlying mechanism for the exacerbated injury in *Gstm1* deficient mice can be explained by increased oxidative stress, as evidenced by elevated kidney ROS levels, and increased 4-

HNE protein adducts and mitochondrial ROS levels in renal tubules. Our *in vitro* studies further support this by showing that treatment with apocynin, an inhibitor of NADPH oxidase, effectively reduces cisplatin-mediated ROS generation, highlighting the involvement of this pathway. Beyond oxidative stress, our data also demonstrate that GSTM1 deficiency augments NF-κB activation and cell death. The observed increase in IL-6 expression in *Gstm1* KO kidneys is consistent with this, as IL-6 is a well-known downstream target of NF-κB signaling. This multifaceted protective role of GSTM1—mitigating oxidative stress, suppressing inflammatory pathways, and reducing cell death—underscores its importance in preserving renal integrity during cisplatin therapy.

These findings have several important clinical implications. First, they provide a strong mechanistic link between GSTM1 and cisplatin nephrotoxicity, identifying GSTM1 as a crucial mediator of cellular defense against this chemotherapeutic agent. Second, our study highlights *GSTM1* null variant as a potential genetic risk factor for increased susceptibility to cisplatin-induced kidney injury in human patients. Third, homozygous *GSTM1* null genotype resulting in complete absence of GSTM1 enzymatic activity is highly prevalent, affecting approximately 40–50% of Caucasian and Asian populations and approximately 27% of African Americans. This means that roughly one in two patients of Caucasian or Asian ancestry receiving cisplatin-based chemotherapy may carry this genetic risk factor, with nearly one in three African American patients similarly affected. The breadth of this prevalence across multiple ethnic groups suggests that *GSTM1* null status is a clinically actionable biomarker candidate of unusually wide reach, distinguishing it from rarer pharmacogenomic variants with more limited population impact. Cisplatin-based regimens are used across a wide range of malignancies (including cancers of the head and neck, lung, ovary, cervix, endometrium, bladder, and testis), meaning that the at-risk population is not restricted to any single cancer type. Establishing *GSTM1* null status as a validated predictive biomarker for cisplatin nephrotoxicity in large cohorts could

therefore inform personalized risk stratification across diverse patient populations and ethnic groups. For example, patients identified as homozygous *GSTM1* null prior to initiating cisplatin therapy could be prioritized for intensified nephroprotective strategies, closer renal function monitoring, or, where oncologically appropriate, consideration of alternative platinum-based agents such as carboplatin, which carries a lower nephrotoxicity burden. Furthermore, the differential prevalence across ethnic groups highlights the importance of inclusive representation in future clinical validation studies, to ensure that any predictive tool derived from this work is equitable and generalizable across populations.

Furthermore, the observation that GSTM1 expression is induced in response to cisplatin suggests that modulating GSTM1 activity or expression could be a viable therapeutic strategy to protect against cisplatin nephrotoxicity. Future research could explore pharmacologic activators of GSTM1 in heterozygous null variant carriers or gene therapy approaches in homozygous null variant carriers to enhance GSTM1 levels in patients at high risk. Targeting the downstream oxidative stress and inflammatory pathways, such as NADPH oxidase or NF-κB, also represents a promising avenue for developing novel renal protective agents in those deficient of GSTM1.

While our study provides robust evidence, it is important to acknowledge certain limitations. The mouse model, while clinically relevant in its dosing regimen, cannot fully replicate the complexity of human physiological responses. Moreover, our bulk kidney mRNA analysis does not allow precise localization of the induction of *Gstm1* to any specific or all nephron compartments. However, IHC analysis reveals GSTM1 protein being most abundantly expressed in the juxtamedullary cortex and outer medullary region and is consistent with RNA-seq data from microdissected nephron segments in the rat. Future studies employing compartment-specific approaches such as laser capture microdissection or single-cell RNA sequencing would more precisely define the cellular distribution of cisplatin-induced *Gstm1* upregulation across nephron segments, and would further strengthen the mechanistic link between proximal tubular *Gstm1*

expression and protection against cisplatin nephrotoxicity. An additional limitation relates to the choice of mouse strain. Our study was conducted in mice on the FVB background, which was selected because the *Gstm1* knockout line was backcrossed onto this strain for over 20 generations, ensuring a congenic background for comparison of wild-type and knockout animals. However, strain-specific differences in susceptibility to cisplatin-induced renal injury and fibrosis are well recognized. Notably, Sears et al. demonstrated that C57BL/6 mice require a higher cisplatin dose than FVB mice to develop renal fibrosis in the repeated low-dose model, establishing FVB as a sensitive strain rather than a resistant one (26). The absence of significant fibrosis in our study, confirmed by Masson's trichrome staining, which showed no significant interstitial fibrosis in either wild-type or *Gstm1* knockout FVB mice at the one-month post-cisplatin time point, is therefore more likely attributable to the relatively early analysis time point, rather than to any intrinsic resistance of the FVB strain to fibrosis. This is particularly noteworthy given the established association between *GSTM1* null variant and CKD progression in humans, where renal fibrosis is a key pathological feature. Future studies employing fibrosis-prone mouse strains, humanized *GSTM1* models, or later post-cisplatin time points would be better positioned to evaluate the specific contribution of GSTM1 deficiency to cisplatin-induced renal fibrosis and would further strengthen the translational relevance of our findings to human CKD progression in *GSTM1* null individuals. Additionally, NF-κB activation was not directly assessed in mouse kidney. p65 immunohistochemistry directly in mouse kidney tissue would provide a more explicit visual link between the nuclear p65 staining observed in GSTM1-deficient human proximal tubular cells *in vitro* and the IL-6 upregulation detected in *Gstm1* knockout kidneys *in vivo*, and represents an important avenue for future investigation in the context of a more comprehensive mechanistic study. We also acknowledge the phylogenetic complexity of the GST mu gene family, which has undergone independent duplications and deletions mice and humans, complicating straightforward ortholog assignment. However, the high degree of sequence conservation between mouse *Gstm1* and human *GSTM1*, their shared

enzymatic activity, concordant renal expression profiles, and the structural similarity of the mouse knockout to the human null deletion collectively support the translational relevance of our model.

Future studies could include larger cohorts and potentially investigate other genetic modifiers that may interact with *GSTM1* to influence susceptibility to cisplatin nephrotoxicity. Additionally, clinical validation of the *GSTM1* null variant as a predictive biomarker in human patient populations is warranted.

In conclusion, our study demonstrates that GSTM1 plays a critical cytoprotective role against cisplatin-induced kidney injury by mitigating oxidative stress, inhibiting NF-κB activation, and reducing cellular apoptosis. These findings significantly advance our understanding of cisplatin nephrotoxicity and highlight the *GSTM1* gene as a potential genetic biomarker for risk stratification and a promising therapeutic target for preventing this devastating side effect of life-saving cancer treatment. Further research is crucial to translate these preclinical findings into clinical strategies to improve outcomes for cancer patients.

Clinical Perspectives

- Cisplatin, a highly effective chemotherapy drug, is significantly limited by kidney injury in up to 30% of patients. This study was undertaken to investigate if the common null variant of the protective enzyme Glutathione-S-transferase Mu-1 (GSTM1) increases susceptibility to this side effect in a mouse model.
- *Gstm1* knockout mice exhibited more severe kidney injury in a clinically relevant low-dose, repeat-cycle cisplatin model, characterized by increased markers of kidney injury, higher reactive oxygen species (ROS) production, and increased inflammation and cell death.

- These findings suggest that the highly prevalent *GSTM1* null genetic variant is a potential risk factor for cisplatin-induced kidney injury in humans, offering a path for personalized risk assessment and the development of targeted preventative or therapeutic strategies to protect kidney health in cancer patients.

Data Availability

The authors declare that all the data supporting the findings in this study are available within the article and its supplementary.

Competing Interests

The authors declare that there are no competing interests associated with this manuscript.

Ethics Approval

All animal experiments were carried out in accordance with local and NIH guidelines, and the animal protocol was approved by the University of Rochester and University of California, Irvine Institutional Animal Care and Use Committees.

Acknowledgment

This work was supported in part by grant R01DK136064 to T.H.L.

Figure Legend

Figure 1. ***Gstm1*** **expression is induced in response to cisplatin treatment in a low dose repeated cisplatin-induced nephropathy mouse model**. (**A**) Schematic representation of experimental design for the mouse model. Low dose cisplatin (9mg/kg) was repeatedly injected intraperitoneally (IP)) once a week for 4 weeks. Mice were sacrificed at the end of 8th week post first cisplatin injection. (**B**) Real time PCR analysis of kidney *Gstm1* expression in cisplatin treated or untreated wild type (WT) mice, normalized to *Gapdh*, (n = 5/group). All data expressed as mean ± SEM; p-values were calculated by unpaired *t*-tests. ** $p < 0.01$. (**C**) Kidney sections of two wild-type mice treated with saline and two wild-type mice treated with cisplatin. Cisplatin significantly induced GSTM1 expression in the juxtamedullary cortex and outer medullary region. Note: due to the high degree of amino acid sequence homology between GSTM1 and GSTM2, the immunohistochemical signal detected by the anti-GSTM1 antibody may reflect combined Mu-class GST expression rather than GSTM1 exclusively, and should be interpreted in conjunction with the isoform-specific qPCR data shown in **Figure 1B**.

Figure 2. **Loss of GSTM1 leads to more severe cisplatin induced kidney injury**. Markers of kidney function were assessed (**A**) Blood urea nitrogen (BUN) (left) and serum creatinine (SCr) (right) were measured from plasma collected at the end of 8 weeks after first cisplatin or vehicle injection (WT + Saline, n = 6; WT + Cisp, n = 11; Gstm1 KO + Cisp, n = 14). (**B**) Left: Quantification of mRNA expression level of the kidney tubular injury marker *Kim-1* normalized to *Gapdh*. n = 11 (WT) and n = 14 (*Gstm1* KO). Middle: Immunohistochemical KIM-1 staining (scale bar, 100 μm). Right:

The KIM-1 stain intensity (a.u) was calculated from five random fields, using image J and presented as a bar graph, n = 5 (WT + Cisp) and n = 4 (KO + Cisp). (**C**) Histological analysis of the kidney section (scale bar = 400 μm). PAS staining and quantification of the kidney injury score was performed by a renal pathologist blinded to experimental conditions and groups, (n = 9-13/group). All data expressed as mean ± SEM; p-values by unpaired *t*-tests. * $p < 0.05$, ** $p < 0.01$.

Figure 3. Cisplatin induces significantly higher level of oxidative stress in *Gstm1* deficient mice.

(**A**) Intracellular ROS measured by DCFDA assay in mouse kidney tissue and expressed as fold change relative to cisplatin-treated wild-type mice. (**B**) Representative Western blot of 4-HNE and GAPDH in kidney lysate from cisplatin-treated wild-type and *Gstm1* KO mice. Total 4-HNE protein adducts were normalized to GAPDH and expressed as fold change relative to cisplatin-treated wild-type mice. WT + Cisp, n = 6; KO + Cisp, n = 8. (**C**) Real time PCR analysis of kidney relative mRNA expression for *Nox2* and *Nox4* (top), and *Il6*, *Mcp-1* and *Tgfβ* (bottom) normalized to *Gapdh*. (**D**) Representative MitoSOX

Red images of primary mouse proximal tubules cells (Scale bar, 100 μm) (left) and mean fluorescence intensity (arbitrary unit (a.u.)) quantified from five random fields and presented as a bar graph (right). (**E**) A representative flow cytometry analysis of Mitochondria ROS; two independent experiments were performed. The representative plots are included as qualitative support for the quantified microscopy data in Panel D.

N = 5 to 11/group. All data expressed as mean ± SEM; p-values by unpaired *t*-tests. * p < 0.05, ** p < 0.01, *** p < 0.001.

Figure 4. Over-expression of GSTM1 in HK-2 cells reduces ROS production in cells treated with cisplatin. (**A**) Intracellular ROS measured by DCFDA in HK-2 control cells and *GSTM1* over-expressed transgenic HK-2 cells (HK2-Tg) treated with cisplatin and with or without the ROS scavenger apocynin. Values are expressed as fold change relative to control. (**B**) Human *NOX2* mRNA expression normalized to *GAPDH* in cisplatin-treated HK-2-control and HK-2-Tg cells. (**C**) Representative MitoSOX Red image (left). Scale bar = 100 μm. Mean fluorescence intensity (arbitrary unit (a.u.)) quantified (right) from five random fields using image J and presented as a bar graph. The data are expressed as mean ± SEM, n= 5 – 6/group; p-values by unpaired *t*-tests; * p < 0.05, ** p < 0.01, *** p < 0.001. (**D**) Representative MitoSOX Red flow-cytometry plots from the same HK-2 cell groups. Two independent flow-cytometry experiments were performed, and the representative plots are included as qualitative support for the quantified microscopy data in Panel C.

Figure 5. **Deletion of GSTM1 leads increased cisplatin induced inflammation and cytotoxicity in HK-2 cells and *Gstm1* KO mice.** (**A**) Representative image for NF-κB p65 immunofluorescence in cisplatin-treated HK-2-control and HK-2-Tg cells (left). Nuclear p65 staining was quantified as the percentage of p65-positive nuclei from at least 150 cells from five random fields per group (graph, right). Two independent experiments were performed. (**B**) Representative Annexin V/7-AAD flow-cytometry

analysis of vehicle- and cisplatin-treated HK-2 control and HK-2-Tg cells (left). Flow cytometry dot plots show Annexin V (x-axis) versus 7-AAD (y-axis) staining. Q1: 7-AAD$^+$/Annexin V$^-$ (membrane-compromised cells without detectable Annexin V staining); Q2: 7-AAD$^+$/Annexin V$^+$ (late apoptotic/necrotic cells); Q3: 7-AAD$^-$/Annexin V$^+$ (early apoptotic cells); Q4: 7-AAD$^-$/Annexin V$^-$ (viable cells). The bar graph (right) quantifies total Annexin V positivity as the combined percentage of early apoptotic (Q3, Annexin V$^+$, 7-AAD$^-$) and late apoptotic/secondary necrotic cells Q2, Annexin V$^+$, 7-AAD$^+$). (**C**) Representative fluorescence images of TUNEL staining in kidney sections from saline- and cisplatin-treated wild-type (WT) and *Gstm1* knockout (KO) mice. Each panel shows DAPI (nuclear stain, blue), TUNEL (green), and merged channels. TUNEL-positive nuclei are virtually absent in saline-treated WT and KO kidneys, establishing a stringent negative baseline. Following repeated low-dose cisplatin treatment, TUNEL-positive nuclei are increased in *Gstm1* KO kidneys compared to WT kidneys, indicating greater DNA fragmentation in the absence of GSTM1. Quantification (right) is expressed as the number of TUNEL-positive cells per field; a total of 150 or more nuclei from five random fields were counted per group. Similar results were obtained from two independent experiments. Scale bar = 100 μm. Quantitation is shown for cisplatin-treated groups only. Data expressed as mean ± SEM, p-values by unpaired *t*-tests. * $p < 0.05$, ** $p < 0.01$.

References

1. Osanto S, Bukman A, Van Hoek F, Sterk PJ, De Laat JA, Hermans J. Long-term effects of chemotherapy in patients with testicular cancer. Journal of clinical oncology : official journal of the American Society of Clinical Oncology. 1992;10(4):574-9.
2. Arany I, Safirstein RL. Cisplatin nephrotoxicity. Semin Nephrol. 2003;23(5):460-4.
3. Berns JS, Ford PA. Renal toxicities of antineoplastic drugs and bone marrow transplantation. Semin Nephrol. 1997;17(1):54-66.
4. Latcha S, Jaimes EA, Patil S, Glezerman IG, Mehta S, Flombaum CD. Long-Term Renal Outcomes after Cisplatin Treatment. Clin J Am Soc Nephrol. 2016;11(7):1173-9.
5. Yao X, Panichpisal K, Kurtzman N, Nugent K. Cisplatin nephrotoxicity: a review. Am J Med Sci. 2007;334(2):115-24.
6. Holditch SJ, Brown CN, Lombardi AM, Nguyen KN, Edelstein CL. Recent Advances in Models, Mechanisms, Biomarkers, and Interventions in Cisplatin-Induced Acute Kidney Injury. Int J Mol Sci. 2019;20(12).
7. McSweeney KR, Gadanec LK, Qaradakhi T, Ali BA, Zulli A, Apostolopoulos V. Mechanisms of Cisplatin-Induced Acute Kidney Injury: Pathological Mechanisms, Pharmacological Interventions, and Genetic Mitigations. Cancers (Basel). 2021;13(7).
8. Atkinson HJ, Babbitt PC. Glutathione transferases are structural and functional outliers in the thioredoxin fold. Biochemistry. 2009;48(46):11108-16.
9. Hayes JD, Flanagan JU, Jowsey IR. Glutathione transferases. Annu Rev Pharmacol Toxicol. 2005;45:51-88.
10. Mannervik B, Board PG, Hayes JD, Listowsky I, Pearson WR. Nomenclature for mammalian soluble glutathione transferases. Methods Enzymol. 2005;401:1-8.
11. Takahashi Y, Campbell EA, Hirata Y, Takayama T, Listowsky I. A basis for differentiating among the multiple human Mu-glutathione S-transferases and molecular cloning of brain GSTM5. J Biol Chem. 1993;268(12):8893-8.
12. Bodonyi-Kovacs G, Ma JZ, Chang J, Lipkowitz MS, Kopp JB, Winkler CA, Le TH. Combined Effects of GSTM1 Null Allele and APOL1 Renal Risk Alleles in CKD Progression in the African American Study of Kidney Disease and Hypertension Trial. J Am Soc Nephrol. 2016;27(10):3140-52.
13. Chang J, Ma JZ, Zeng Q, Cechova S, Gantz A, Nievergelt C, et al. Loss of GSTM1, a NRF2 target, is associated with accelerated progression of hypertensive kidney disease in the African American Study of Kidney Disease (AASK). Am J Physiol Renal Physiol. 2013;304(4):F348-55.
14. Le TH. GSTM1 Gene, Diet, and Kidney Disease: Implication for Precision Medicine?: Recent Advances in Hypertension. Hypertension. 2021;78(4):936-45.
15. Levy R, Le TH. Role of GSTM1 in Hypertension, CKD, and Related Diseases across the Life Span. Kidney360. 2022;3(12):2153-63.
16. Levy RV, Reidy KJ, Le TH, David V, Winkler C, Xu Y, et al. Association of GSTM1 Deletion With Progression of CKD in Children: Findings From the Chronic Kidney Disease in Children (CKiD) Study. Am J Kidney Dis. 2021.
17. Tin A, Scharpf R, Estrella MM, Yu B, Grove ML, Chang PP, et al. The Loss of GSTM1 Associates with Kidney Failure and Heart Failure. J Am Soc Nephrol. 2017;28(11):3345-52.
18. Gigliotti JC, Tin A, Pourafshar S, Cechova S, Wang YT, Sung SJ, et al. GSTM1 Deletion Exaggerates Kidney Injury in Experimental Mouse Models and Confers the Protective Effect of Cruciferous Vegetables in Mice and Humans. J Am Soc Nephrol. 2020;31(1):102-16.

19. Li P, Li D, Lu Y, Pan S, Cheng F, Li S, et al. GSTT1/GSTM1 deficiency aggravated cisplatin-induced acute kidney injury via ROS-triggered ferroptosis. Front Immunol. 2024;15:1457230.
20. Sharp CN, Doll MA, Megyesi J, Oropilla GB, Beverly LJ, Siskind LJ. Subclinical kidney injury induced by repeated cisplatin administration results in progressive chronic kidney disease. Am J Physiol Renal Physiol. 2018;315(1):F161-F72.
21. Ding W, Yousefi K, Shehadeh LA. Isolation, Characterization, And High Throughput Extracellular Flux Analysis of Mouse Primary Renal Tubular Epithelial Cells. J Vis Exp. 2018(136).
22. Salzler HR, Griffiths R, Ruiz P, Chi L, Frey C, Marchuk DA, et al. Hypertension and albuminuria in chronic kidney disease mapped to a mouse chromosome 11 locus. Kidney Int. 2007;72(10):1226-32.
23. Yang Y, Parsons KK, Chi L, Malakauskas SM, Le TH. Glutathione S-transferase-micro1 regulates vascular smooth muscle cell proliferation, migration, and oxidative stress. Hypertension. 2009;54(6):1360-8.
24. Pabla N, Dong Z. Cisplatin nephrotoxicity: mechanisms and renoprotective strategies. Kidney Int. 2008;73(9):994-1007.
25. Gil da Costa RM, Levesque C, Bianchi-Frias D, Chatterjee P, Lam HM, Santos C, et al. Pharmacological NF-kappaB inhibition decreases cisplatin chemoresistance in muscle-invasive bladder cancer and reduces cisplatin-induced toxicities. Mol Oncol. 2023;17(12):2709-27.
26. Sears SM, Sharp CN, Krueger A, Oropilla GB, Klinge CM, Schnellmann RG, Siskind LJ. C57BL/6 mice require a higher dose of cisplatin to induce renal fibrosis and CCL2 correlates with cisplatin-induced kidney injury. Am J Physiol Renal Physiol. 2020;319(4):F674–F685.

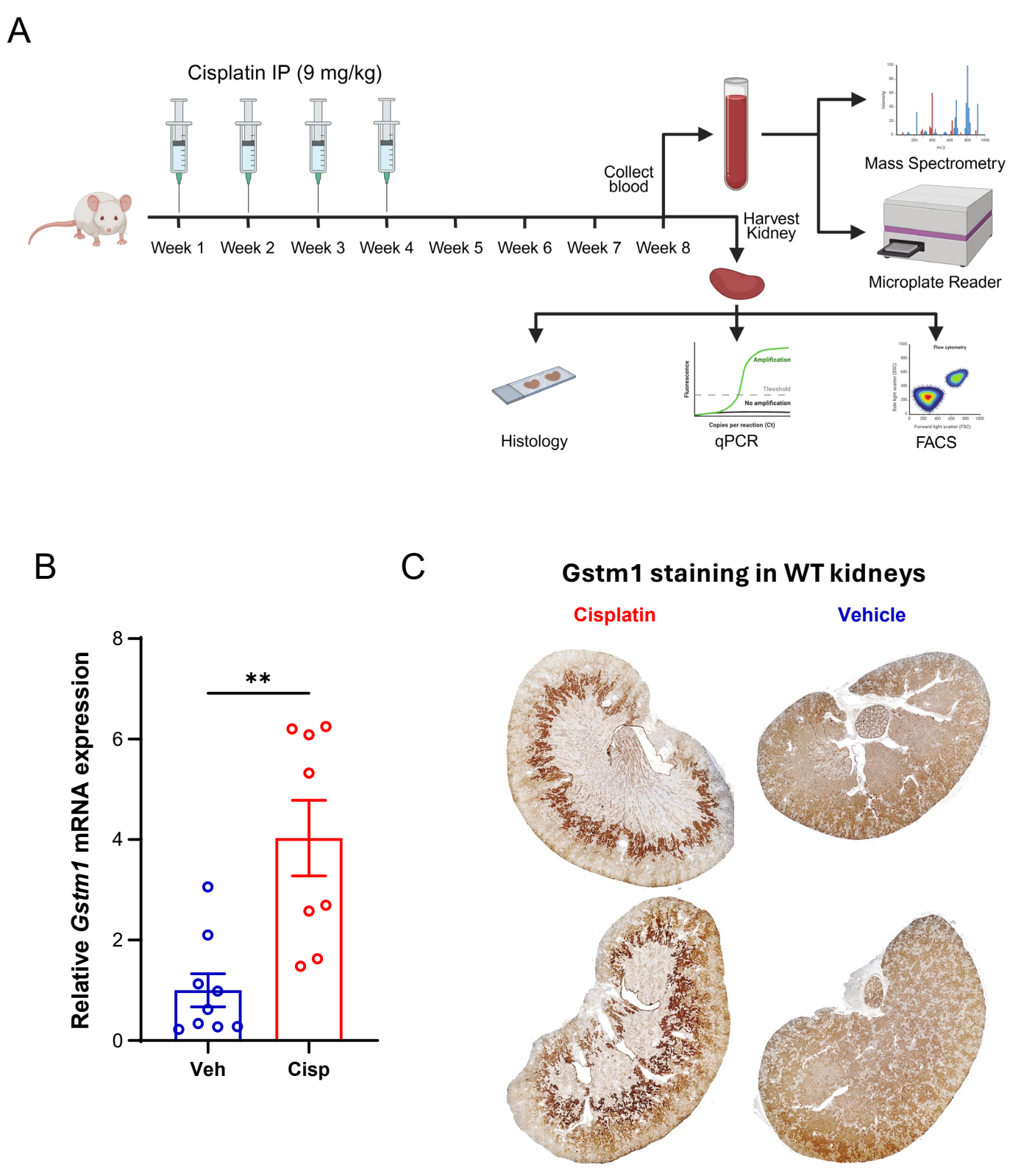

A
Cisplatin IP (9 mg/kg)
Week 1
Week 2
Week 3
Week 4
Week 5
Week 6
Week 7
Week 8
Collect blood
Harvest Kidney
Mass Spectrometry
Microplate Reader
Histology
qPCR
FACS
B
Relative Gstm1 mRNA expression
**
Veh
Cisp
C
Gstm1 staining in WT kidneys
Cisplatin
Vehicle

Figure 1

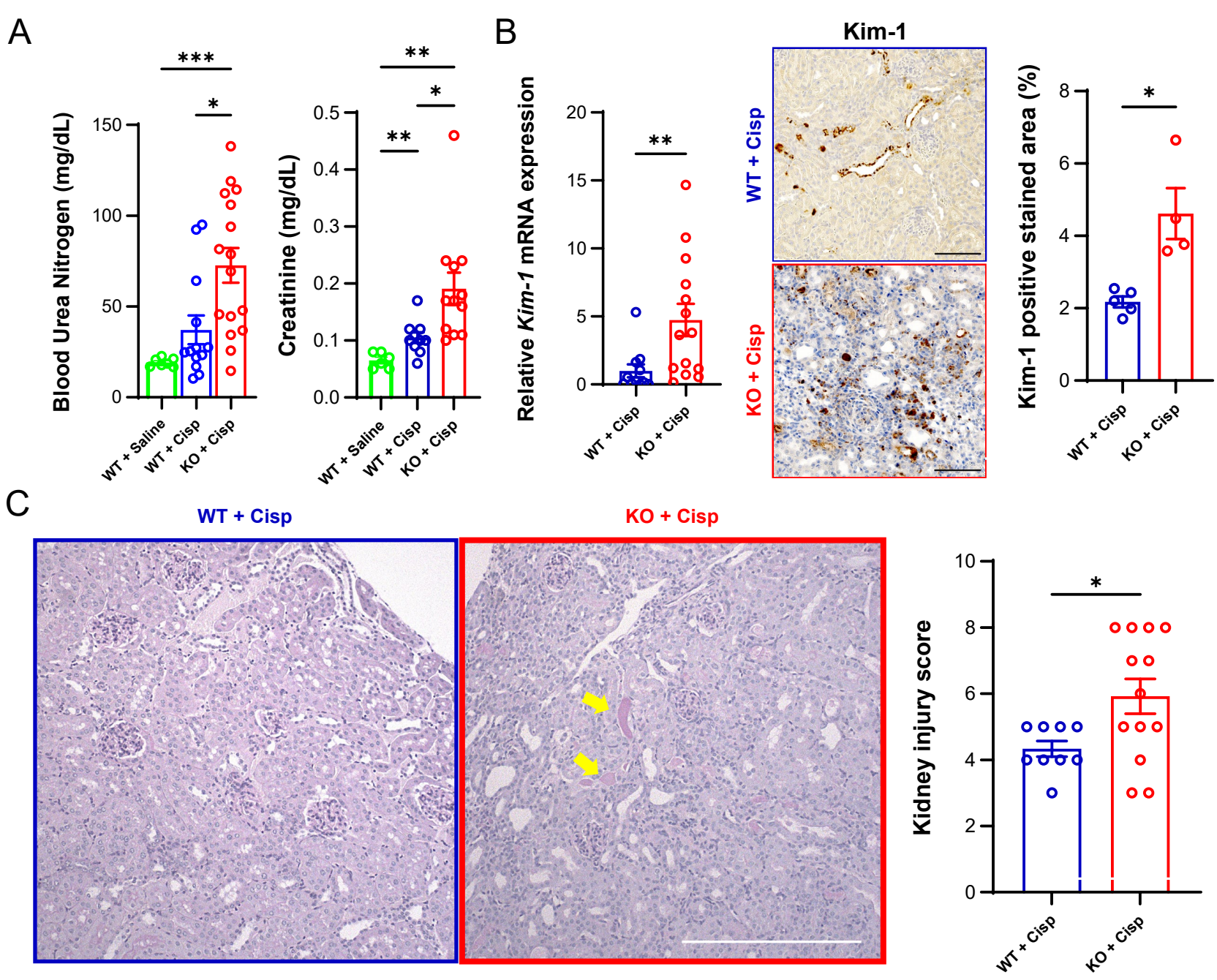
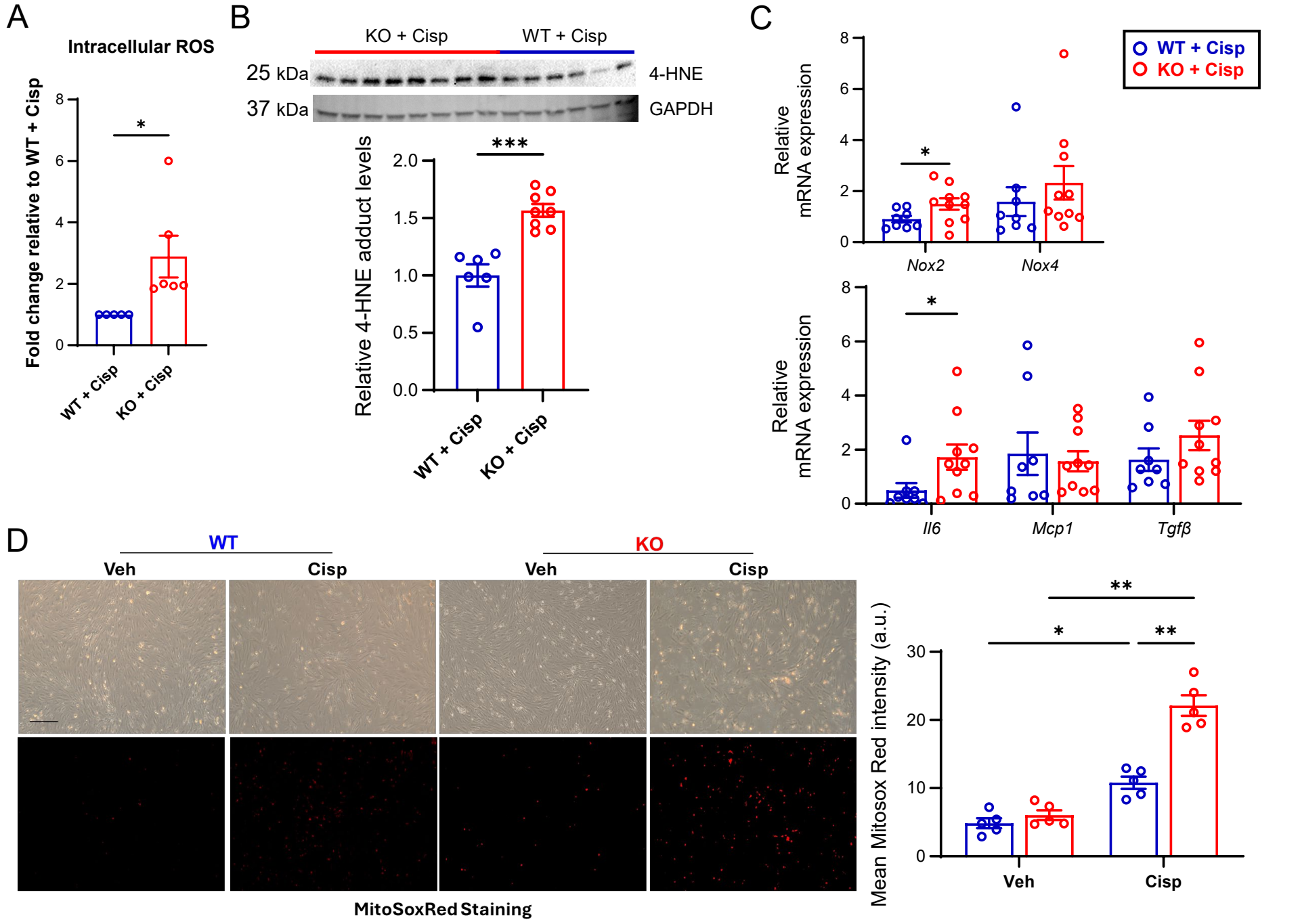

A
Blood Urea Nitrogen (mg/dL)
150
100
50
0
***
*
WT + Saline
WT + Cisp
KO + Cisp
Creatinine (mg/dL)
0.5
0.4
0.3
0.2
0.1
0.0
**
**
*
WT + Saline
WT + Cisp
KO + Cisp
B
Relative Kim-1 mRNA expression
20
15
10
5
0
**
WT + Cisp
KO + Cisp
Kim-1
WT + Cisp
KO + Cisp
Kim-1 positive stained area (%)
8
6
4
2
0
*
WT + Cisp
KO + Cisp
C
WT + Cisp
KO + Cisp
Kidney injury score
10
8
6
4
2
0
*
WT + Cisp
KO + Cisp

Figure 2


A
Intracellular ROS
Fold change relative to WT + Cisp
WT + Cisp
KO + Cisp
B
KO + Cisp
WT + Cisp
25 kDa
4-HNE
37 kDa
GAPDH
Relative 4-HNE adduct levels
C
WT + Cisp
KO + Cisp
Relative mRNA expression
Nox2
Nox4
Il6
Mcp1
Tgfβ
D
WT
KO
Veh
Cisp
MitoSoxRed Staining
Mean Mitosox Red intensity (a.u.)

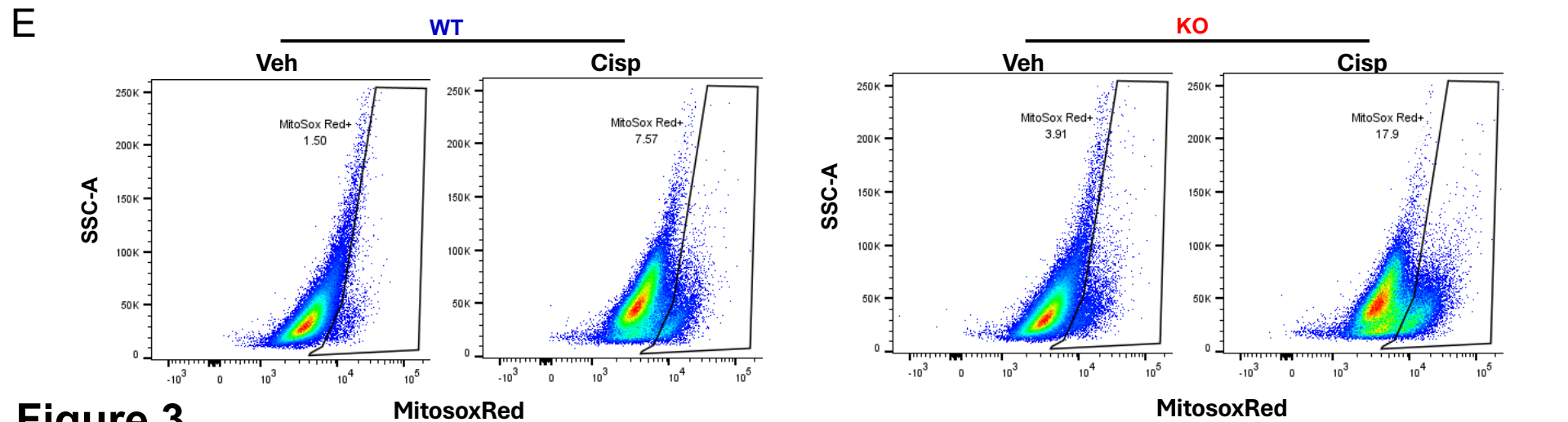

E
WT
KO
Veh
Cisp
SSC-A
MitoSox Red+
1.50
7.57
3.91
17.9
MitosoxRed

Figure 3

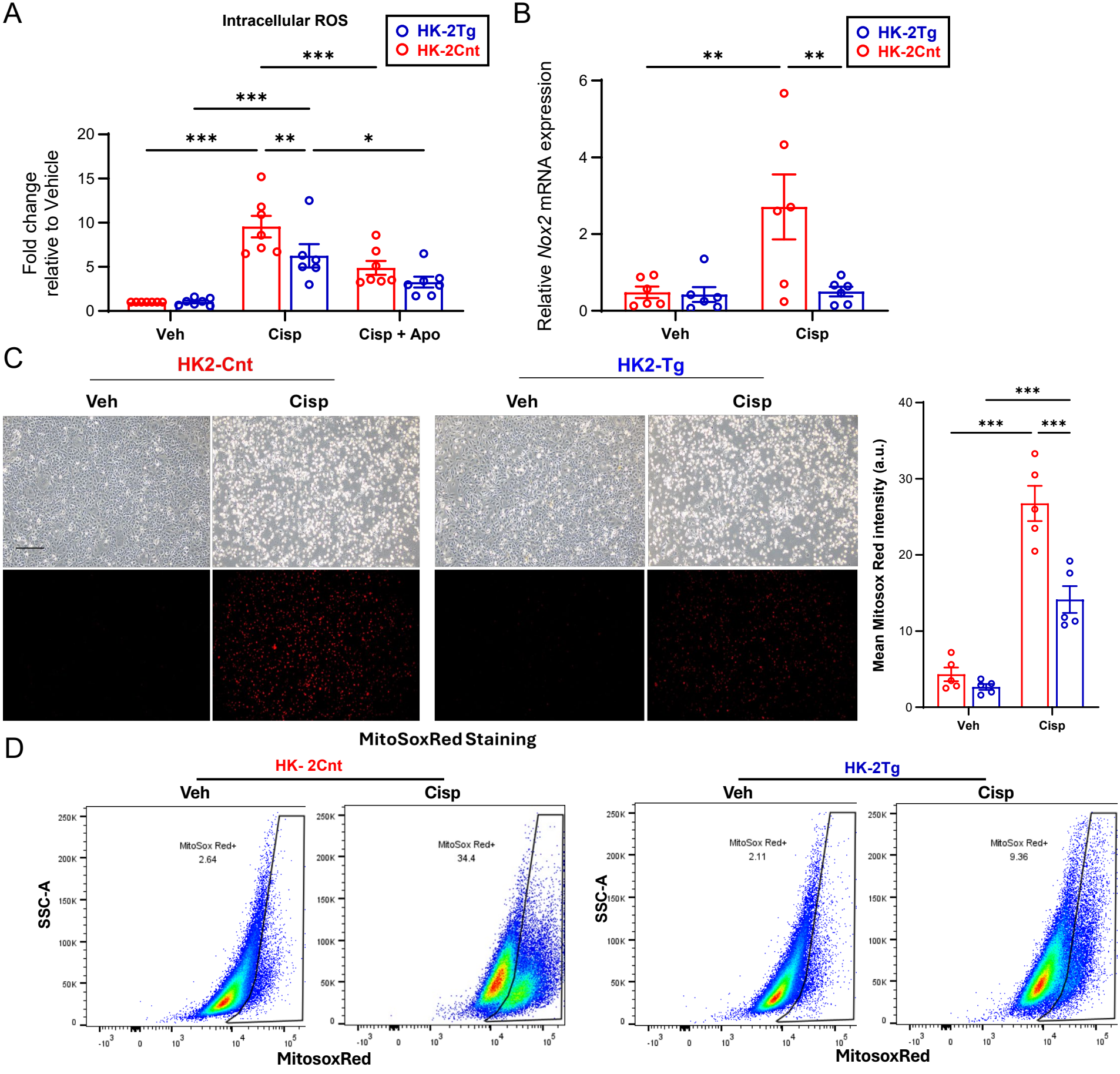

A
Intracellular ROS
HK-2Tg
HK-2Cnt
***
***
***
**
*
Fold change relative to Vehicle
20
15
10
5
0
Veh
Cisp
Cisp + Apo
B
HK-2Tg
HK-2Cnt
**
**
Relative Nox2 mRNA expression
6
4
2
0
Veh
Cisp
C
HK2-Cnt
HK2-Tg
Veh
Cisp
Veh
Cisp
***
***
***
Mean Mitosox Red intensity (a.u.)
40
30
20
10
0
Veh
Cisp
MitoSoxRed Staining
D
HK- 2Cnt
HK-2Tg
Veh
Cisp
Veh
Cisp
MitoSox Red+
2.64
MitoSox Red+
34.4
MitoSox Red+
2.11
MitoSox Red+
9.36
SSC-A
250K
200K
150K
100K
50K
0
-10^3
0
10^3
10^4
10^5
MitosoxRed

Figure 4

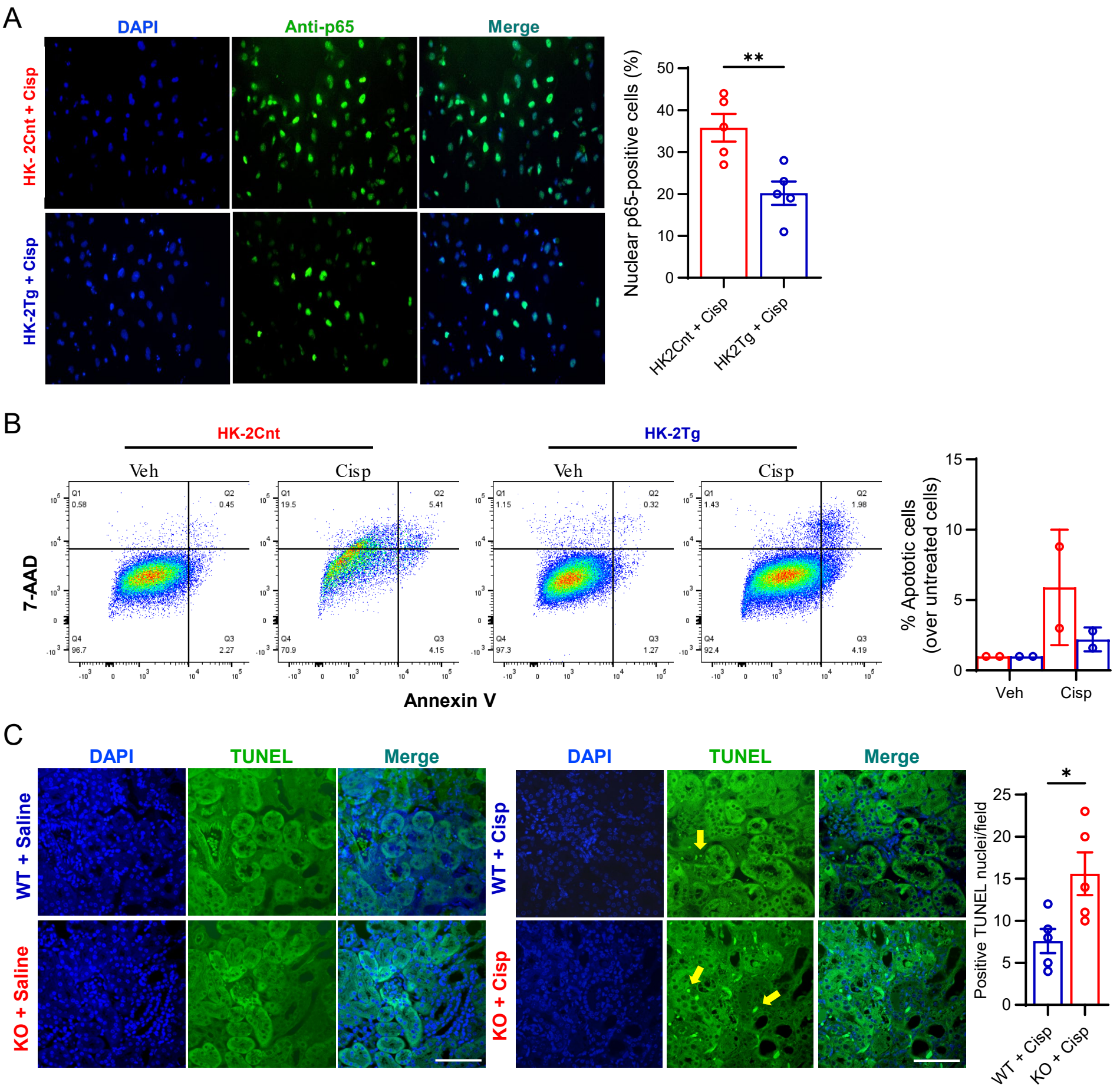

A
DAPI
Anti-p65
Merge
HK- 2Cnt + Cisp
HK-2Tg + Cisp
Nuclear p65-positive cells (%)
**
HK2Cnt + Cisp
HK2Tg + Cisp
B
HK-2Cnt
HK-2Tg
Veh
Cisp
7-AAD
Annexin V
% Apototic cells (over untreated cells)
C
DAPI
TUNEL
Merge
WT + Saline
KO + Saline
WT + Cisp
KO + Cisp
Positive TUNEL nuclei/field
*

Figure 5